Research Article | Vol. 27, No. 8 | 15 Apr 2019 | OPTICS EXPRESS A524
Optics EXPRESS

Broadband antireflection Mie scatterers revisited—a solar cell and module analysis

LAURA STEVENS,[1,*] NICO TUCHER,[1,2] OLIVER HÖHN,[1] HUBERT HAUSER,[1] CLAAS MÜLLER,[3] AND BENEDIKT BLÄSI[1]

[1]*Fraunhofer ISE, Heidenhofstr. 2, 79110 Freiburg, Germany*
[2]*University of Freiburg, Department of Sustainable Systems Engineering INATECH, Georges-Köhler-Allee 103, 79110 Freiburg, Germany*
[3]*University of Freiburg, Department of Microsystems Engineering IMTEK, Georges-Köhler-Allee 103, 79110 Freiburg, Germany*
[*]*laura.stevens@ise.fraunhofer.de*

Reflectance, reduction, and light trapping enhancement are essential to maximize the absorption of silicon solar cells. The industrial state of the art method to improve the solar cell optics is wet chemical texturization of the front surface in combination with the deposition of antireflection coatings. This work analyzes an alternative route, namely a TiO_2 pillar structure on the front side of a planar silicon solar cell encapsulated in ethylene vinyl acetate (EVA) and glass. It focuses on parameter variations of the structured TiO_2 layer while taking the module encapsulation into account. It is shown that internal reflections at the front interface of the module play a crucial role for the structure design. This leads to optimized structures working in a different optical regime. While state of the art structures optimized for a half infinite encapsulation act as effective media, structures optimized for the full module show an improved performance by making use of diffractive effects. It could be shown that weighted reflectance of 4.7% can be reached for a solar module with TiO_2 pillar structure on top of the silicon surface compared to 5.5% for a two-layer ARC with a TiO_2 bottom layer and 2.3% for an isotexture, which is the state of the art structure for multicrystalline silicon cells.

1. Introduction

For industrially relevant silicon solar cells with a thickness of 200 µm or less [1], strong light coupling into the silicon as well as good light trapping is essential to maximize the energy conversion efficiency. Surface texturing in combination with antireflection coatings typically fulfills these requirements in silicon photovoltaics [2]. In industry, texturing is predominantly realized by wet chemical etching processes. Monocrystalline silicon is typically etched with an alkaline etching medium, which leads to randomly arranged pyramidal structures [3]. Multicrystalline silicon wafers are textured using an isotropic etching process based on an aqueous solution of HF/HNO_3, which results in the so called isotexture [4].

Stochastic sub-micron texturing schemes, e.g. black silicon formed by reactive ion etching [5,6] or using metal assisted (wet chemical) etching (MAE) [7], are alternative approaches for multicrystalline silicon. Critical issues within the latter process that are challenging for an industrial realization are the cleaning and removal of metal particles. Also template based etching processes where studied extensively. Etching masks can be patterned by photolithography [8], inkjet printing [9], laser ablation [10], nanoimprint lithography (NIL) [11] or colloidal masks [12]. There are studies about nano-cone antireflection textures directly realized in the high index material silicon [13,14]. Furthermore, Brongersma et al. [15] point out that in terms of photonic effects and resonances, it is of advantage to realize surface structures consisting of high index materials such as silicon.

#355787 https://doi.org/10.1364/OE.27.00A524
Journal © 2019 Received 20 Dec 2018; revised 14 Mar 2019; accepted 15 Mar 2019; published 4 Apr 2019

Optics EXPRESS

One specific defined texture etched into silicon was presented by Spinelli et al., leading to broadband antireflection Mie scattering [16]. These structures reduce reflectance by light scattering and coupling towards the substrate. With these photonic structures excellent optical properties were reported.

All approaches mentioned so far rely on a texturing of the silicon substrate, which leads to an enlargement of the surface area and thereby to an increased surface recombination. This influences the open circuit voltage, which is higher for a planar standard passivated silicon solar cell than for a structured one [17]. One idea avoiding this surface enlargement is the application of an optically functional surface onto a planar electrically passivated surface, which again was introduced by Spinelli et al. [18]. In this work, they showed that much higher minority carrier lifetimes can be achieved with a patterned TiO_2 layer on top of planar silicon than for structures etched into silicon. Such an electrically planar, but optically structured (EPOS) interface on final device level was first demonstrated for rear side gratings by Eisenlohr et al. [19,20] and later also applied to achieve a record efficiency in a silicon-based multijunction solar cell [21].

In a later work, Spinelli et al. compared the optical performance of nanopillars etched into silicon with TiO_2 nanopillars formed by nanoimprint lithography (NIL) in a solar module [22]. Similar work was done by Goldman et al. [23] for InP wafers. Again, the optical performance of the structures etched into silicon outperforms the ones formed into TiO_2. However, a holistic model-based design of the TiO_2 pattern was not possible in their work since they did not include reflection at the front side of the module glass in their model.

Within the present work, we take on that approach of Spinelli et al. and therefore chose the title of the paper in reference to their works. We carry on their concept by taking into account the full module stack (especially the glass-air-interface at the front side), when studying different types of structures. This seems like an incremental addition but it turns out to strongly change the design criteria for the implementation of a photonic structure. In section 2, rigorous coupled wave analysis (RCWA) [24] is used for the modeling of the reflectance of the solar cell front side with half infinite encapsulation and half infinite bulk. To simulate a solar cell in a module stack, a first order correction [25] of these results is shown in section 3. A simulation of the full module stack with the RCWA in combination with the OPTOS (optical properties of textured optical sheets) approach [26], a matrix-based formalism to determine the optical properties of textured optical surfaces, is presented in section 4. Here, OPTOS is used to design and assess light trapping structures based on a nanostructured TiO_2 sol-gel layer for the application in a solar module.

2. Modeling the reflectance of the solar cell front side

The system investigated at first consists of a silicon substrate semi-infinite thickness covered with a 5 nm thick Al_2O_3 passivation layer and a structured TiO_2 sol-gel layer ($n = 2.25$ at 500 nm [27]). In order to obtain relevant results for the module case, a semi-infinite encapsulation layer from the top by a material with a constant refractive index of $n_{EVA} = 1.5$, as an absorption free representation of the encapsulation material ethylene vinyl acetate (EVA) and of the cover glass ($n_{Glass} = 1.5$) is used. As the refractive indices of EVA and the front glass are assumed to be equal, they are modeled as one single layer – the encapsulation – throughout the rest of the work. The investigated photonic structure is a binary crossed grating of TiO_2 pillars with a defined residual layer of TiO_2 – the same structure that was considered by Spinelli [22].

The height of the structure, the diameter of the pillars, the period and the residual layer thickness are varied. A sketch of the simulated structure including the optically relevant layers and a description of the parameters is shown in Fig. 1. The 5 nm thick Al_2O_3, layer, which has a negligible optical effect is omitted in the sketch for simplicity.

Optics EXPRESS

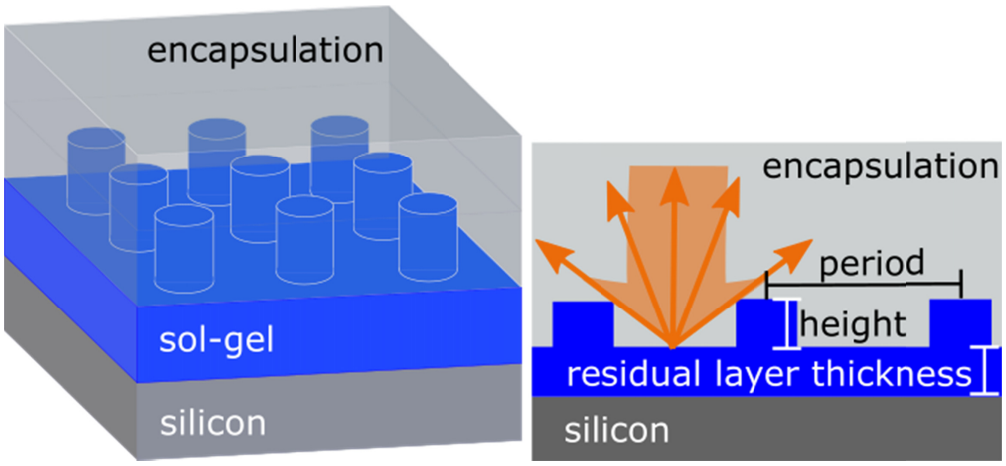

Fig. 1. 3D-Plot and cross sectional sketch of simulated pillar structure. Parameter variations were performed for height, diameter, period and residual layer thickness.

In order to simplify the presentation of the results, the geometrical filling factor FF was used for the structured layer. It is defined as the ratio of the area consisting of TiO_2 (A_{TiO2}) to the area of the simulated unit cell ($A_{unitcell}$):

$$FF = \frac{A_{TiO_2}}{A_{unitcell}}. \quad (1)$$

The resulting reflectance at the solar cell respectively module front is weighted with the photon flux in the AM1.5g spectrum [28] in the wavelength range from 400 nm to 1200 nm. The escape contribution of the cell backside to the overall module reflectance is not taken into account, because a semi-infinite silicon bulk is used for the modelling. The refractive index data of the TiO_2 was taken from experimental data published in [27]. For evaluating the overall performance of the whole module stack, the photon flux absorbed within the silicon is integrated to calculate a photo current density [29].

Results without residual layer

The simulation results of the mentioned system with a structure height of 80 nm and no residual layer for varying filling factors FF and different periods is shown in the left part of Fig. 2. The results show that the reflectance depends strongly on the filling factor. The highest weighted reflectance is obtained for a filling factor of zero. Furthermore, a lower reflectance is reached for high filling factors. Without a residual layer the optimal system in terms of reflectance is a planar layer of TiO_2. Note that the silicon is encapsulated by EVA, which leads to a weighted reflectance of 19.2% without any TiO_2. This is lower than the well-known value of 36% for silicon in air. Modeling a state of the art isotexture as described in [30] with semi-infinite encapsulation at the front side and an 80 nm thick silicon-nitride layer on top of the structure. It leads to a weighted reflectance of 4.3%.

A simulation study for a wider parameter range (structure heights from 40 nm up to 100 nm, residual layer thicknesses from 0 nm to 80 nm) showed a strong influence of the residual layer thickness. Within this parameter variation, a residual layer thickness of 60 nm in combination with a structure height of 80 nm leads to the best reflectance results. Thus, in the following these parameters are kept constant.

Optics EXPRESS

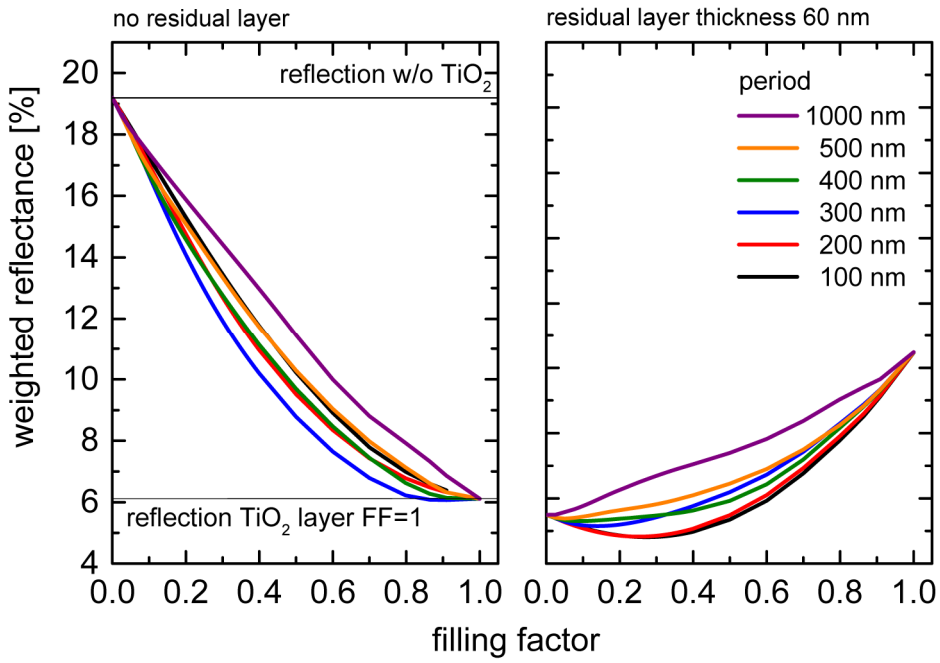

Fig. 2. Weighted reflectance for a system of a structured TiO_2 layer with a fixed height of 80 nm as function of the filling factor. Left: System without a residual layer. The smallest weighted reflectance is reached for filling factors 0.9. Right: System with residual layer thickness of 60 nm. Small periods (100 nm and 200 nm) lead to the smallest reflectance.

Results with a residual layer thickness of 60 nm

A comparison of the weighted reflectance results for a system with a fixed residual layer thickness of 60 nm and a fixed structure height of 80 nm in dependence of the filling factor for different periods is shown in Fig. 2 on the right. The weighted reflectance (R_w) here is smallest for small filling factors. The minimum weighted reflectance with a value of 4.8% is reached in the filling factor range between 0.225 and 0.25 for small periods such as 100 nm and 200 nm. These results are close to the results from Spinelli et al. [22] where the best results with 4.2% reflectance were reached for structures with a diameter of 120 nm, a height of 80 nm, a residual layer thickness of 65 nm and a period of 200 nm. The reached minimal reflectance is slightly lower compared to an optimized flat TiO_2 layer on top of the silicon substrate, with a reflectance is 5.4% for a layer thickness of 65 nm.

These optimal structure parameters are much smaller than the wavelength of the incoming light, thus no higher diffraction orders can propagate. This is important as a low reflectance alone is not sufficient to lead to a large absorption within the silicon wafer. In the long wavelength range additionally a good light redistribution performance is necessary. The optimized structure was therefore compared to a planar two-layer antireflection coating (residual layer + modulated region treated as an effective medium), which was modeled using a transfer matrix method. The refractive index of the structured layer was determined by effective medium theory (EMT). A comparison of different EMT approaches was performed [31–33], which includes the linear weighting of the refractive indices introduced by Birchak et al [34], also referred to as “parallel model” [31], the Drude / Volume Averaging Theory (VAT) [32], the Series [32], the Lorentz-Lorenz [31], the Maxwell-Garnett Theory (MGT) [32] and the Bruggeman theory [35]. The best agreement with the RCWA results was achieved with the Bruggeman theory:

Optics EXPRESS

$$b = (3 \cdot FF - 1) \cdot n^2_{TiO_2} + (2 - 3 \cdot FF) \cdot n^2_{EVA}$$
$$n_{effective} = \sqrt{\frac{b + \sqrt{8 \cdot n^2_{EVA} \cdot n^2_{TiO_2} + b^2}}{4}} \quad (2)$$

in which FF is the geometrical filling factor.

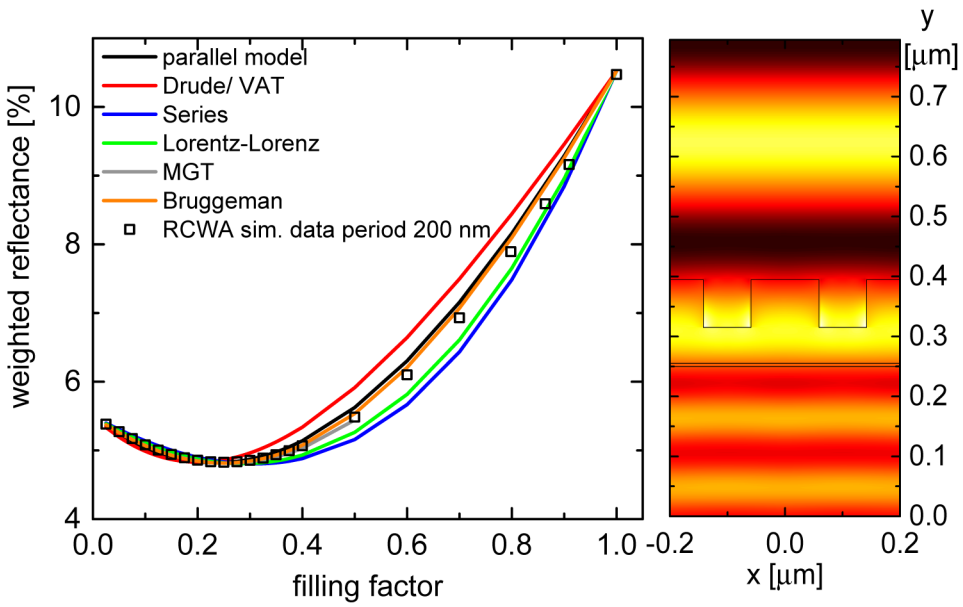

Fig. 3. Left: Comparison of the RCWA simulation results for a structure with period 200 nm, height 80 nm and residual layer thickness 60 nm with the results from the different effective medium models. The best agreement between the RCWA simulation results and an effective medium model was reached for the Bruggeman model. For small filling factors the simulation data fits perfectly to the Bruggeman model. Right: A near field analysis showing two periods of a structure with an height of 80 nm and residual layer thickness of 60 nm, a 5 nm thick passivation layer of Al_2O_3 for wavelength 500 nm. It is clear to see that the wave front passes nearly unperturbed through the structure.

The comparison between the RCWA simulation for the period of 200 nm and the different effective medium models is shown in Fig. 3. The Bruggeman result fits very well to the RCWA simulation data. Please note that this is a phenomenological comparison of exemplary EMTs. An in-depth analysis of the reason why Bruggeman is closest to the RCWA results is beyond the scope of this work.

The diffraction orders in transmission into the silicon half space for a period of 200 nm were also evaluated and show zero efficiency for higher orders. In the near field plot for a structure with a height of 80 nm, a residual layer of 60 nm, a 5 nm thick passivation layer of Al_2O_3 for wavelength 500 nm on the right side in Fig. 3 it is evident that the wave front passes nearly unperturbed through the structure. This confirms that the system can be described as an effective two-layer antireflection coating, where the bottom layer is TiO_2 and the top layer has a refractive index of around 1.69. Hence, for this configuration the structuring has no additional benefit. Comparing this finding with the results published by Spinelli et al. [22], it can be said, that these specific structures in EVA are no Mie scatterers; they behave as an effective two-layer antireflection coating.

Optics EXPRESS

3. Modeling the reflectance of a full solar module stack – First order correction

As the final device is a solar module, the focus of all further investigations will be placed on the scenario with an encapsulation and air as medium in the upper half space. Tracing the angles of the reflected light and binning the corresponding intensities leads to the cases of (i) total internal reflection and (ii) outcoupling at the encapsulation-air-interface. The encapsulation-air-interface leads to total internal reflectance above the critical angle of $\vartheta = 41.8°$, which reduces outcoupling and can help to further decrease the overall reflectance especially for systems with a larger period. In Fig. 4 a sketch of the described structure and possible light paths is shown.

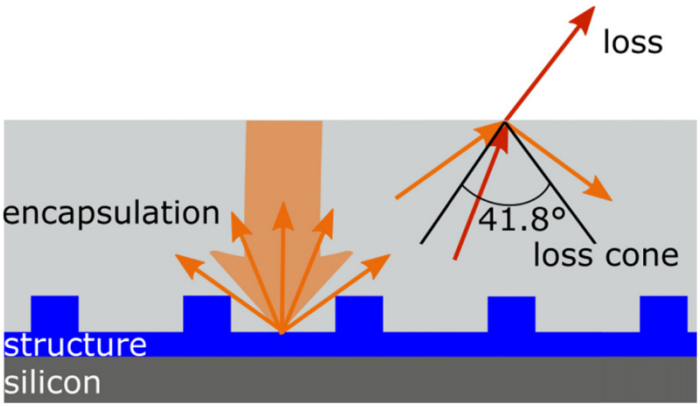

Fig. 4. Sketch of the modeled system of a sol-gel structured solar module. The structure is placed on a semi-infinite silicon substrate at the backside and at the front side an encapsulation with an interface to air. Incoming light is reflected at the structure. The encapsulation-air-interface leads to total internal reflection above the critical angle of $\vartheta < 41.8°$, which could help to further decrease reflectance for the systems with a larger period.

At first, a first order correction is applied to the results discussed above. This means, that light, which is diffracted back at the encapsulation-structure-interface at angles smaller than 41.8 ° can escape and is regarded as lost as in the model applied so far. But light diffracted back at larger angles will experience total internal reflection at the encapsulation-air-interface. This light is counted completely as absorption in the silicon solar cell. No further light paths are assumed. If this in the first order approximation is taken into account, larger periods become interesting again, as diffraction only occurs for reasonably large periodic structures. In comparison to the results shown in the section 2, the diagram in Fig. 5 shows the summed weighted reflectance (triangles) for the periods 500 nm, 600 nm and 700 nm, the weighted reflectance for $\vartheta < 41.8°$, which represents the losses (squares), and in addition for $\vartheta > 41.8°$ (dots).

Optics EXPRESS

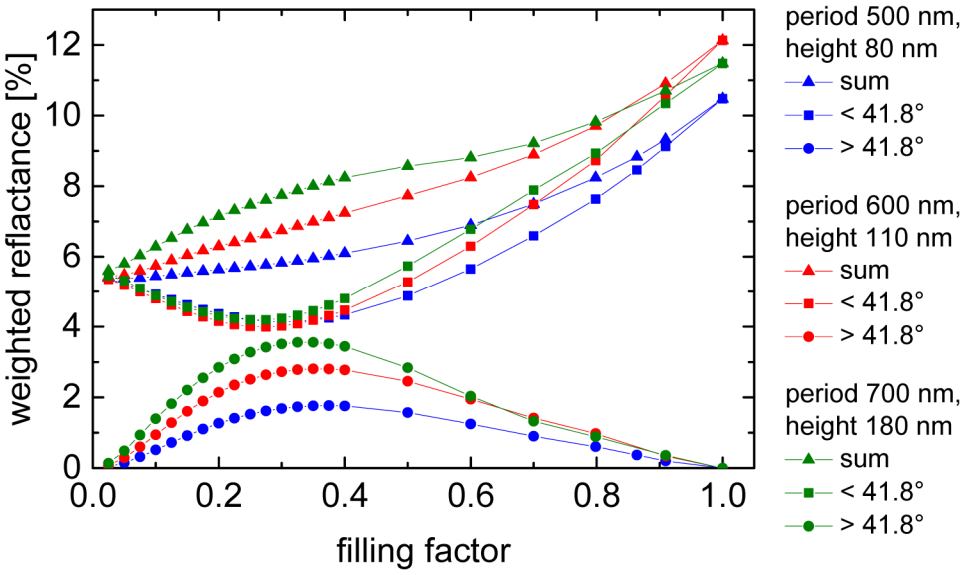

Fig. 5. The modeled weighted reflectance for a pillar structure with a residual layer thickness of 60 nm, periods of 500 nm, 600 nm and 700 nm (triangles). In squares the weighted reflectance for angles smaller than 41.8° is shown and in dots for angles greater than 41.8°. The minimum in the reflectance for angles smaller than 41.8° is reached for a structure with a period of 600 nm and of height of 110 nm.

For very small as well as for high filling factors no gain by differentiating the reflectance in different angular ranges is observed, because diffraction orders other than the 0th order carry only very little energy. In these parameter ranges the functional structure elements (thin cylinders or narrow holes) are so small that they hardly interact with the incident light. For filling factors up to 0.4 the results for $\vartheta < 41.8°$ are for all periods very close. The lowest weighted reflectance R_w ($\vartheta < 41.8°$) with 4.0% is reached for structures with a period of 600 nm, a height of 110 nm and a filling factor of 0.275. In a module, where the front interface is taken into account, this approximation indicates that the structure performs better than the effective two layer structure explained above with a reflectance of 4.8%.

4. Modeling solar module stack accounting for multiple light interactions

In a real photovoltaic module stack, light, which is reflected back at the encapsulation-air-interface has the chance to be absorbed in the solar cell, but also multiple interactions are in principle possible (Fig. 6). Furthermore, a part of the light within the escape cone ($\vartheta < 41.8°$) will be reflected at the encapsulation-air-interface and directed back towards the solar cell.

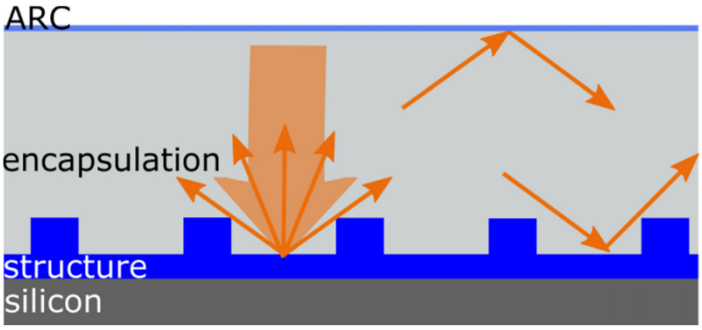

Fig. 6. Sketch of the module with multiple light interactions used in the OPTOS formalism. The EVA is covered with an ARC to reduce reflectance on the module front side.

To take these multiple interactions into account, the OPTOS formalism [26], which utilizes data generated with the RCWA method, was used. The modeled system also includes an antireflection coating (thickness 130 nm, n = 1.27 [36]) on top of the module encapsulation. Note that the displayed reflectance results in Fig. 5 still only consider the module front side reflectance and do not take into account the escape contribution of the back side of the module.

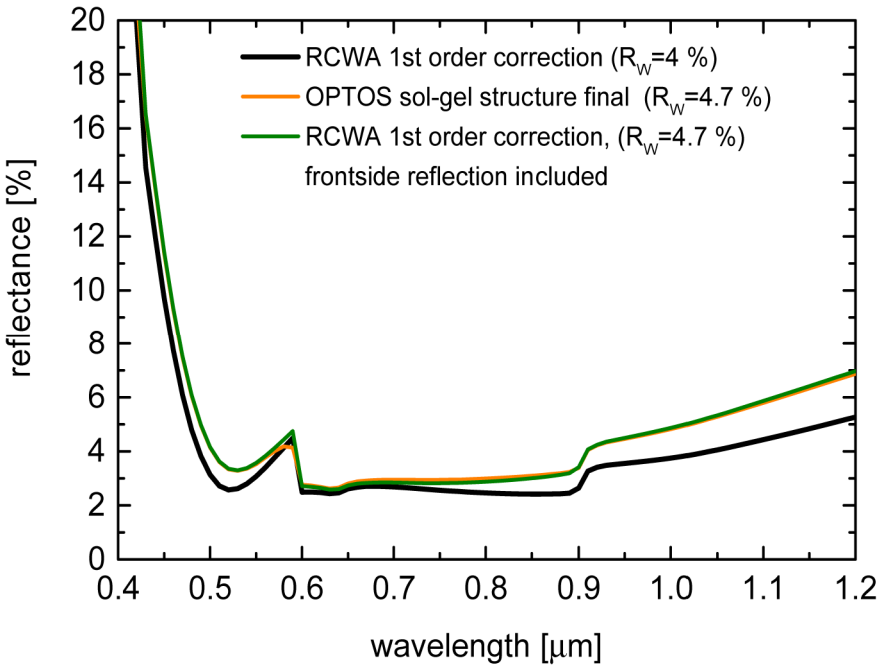

Fig. 7. Comparison between the simulation results of the RCWA and the OPTOS formalism. The RCWA first order correction used in the optimization above is close to the OPTOS results. If reflectance at the front glass is taken into account the corrected RCWA results fit very well to the OPTOS simulation.

The first order corrected results as used in the optimization above qualitatively resemble to the OPTOS results (shown in Fig. 7). However for the smaller and higher wavelength the RCWA first order correction results show a smaller reflectance. The reason is that in the RCWA modeling no reflectance at a module front glass for incident light was taken into account. The corrected result is shown in green and it fits very well to the OPTOS simulation results. So the approximation of a module stack reflectance by summing all angles $\vartheta < 41.8°$

as loss is very good and can be applied in further optimizations without the need for a complete OPTOS calculation.

It is interesting to observe that the reflectance curves show two kinks. Coming from the long wavelength side, higher diffraction orders start propagating in the encapsulation at 900 nm, leading to a reduced reflectance due to total internal reflection at the encapsulation-air-interface. For wavelengths < 600 nm higher diffraction orders can propagate in air, leading to an enhanced outcoupling below this wavelength.

Finally, the optimized sol-gel-structure, the optimized two-layer ARC mentioned above, and an isotexture with an 80 nm thick SiN antireflection layer are compared (Fig. 8). The two-layer ARC is the result of the optimization with the boundary conditions explained in section 2.

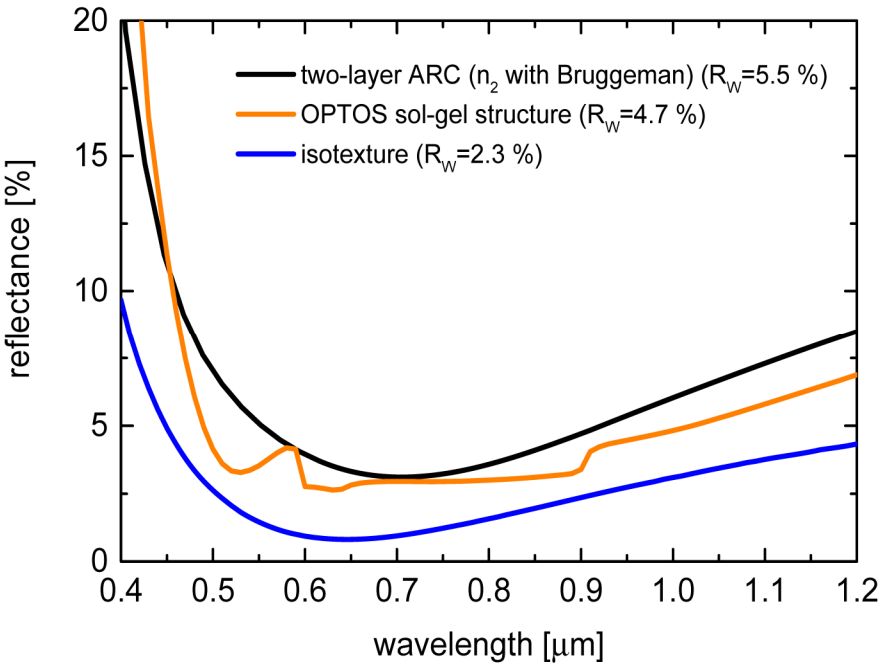

Fig. 8. Comparison of the sol-gel structure (OPTOS results) with a two-layer antireflection coating and an isotexture. The reflectance is shown in dependence of the wavelength. All results are determined in a module stack case. The lowest reflectance over the complete wavelength range is reached for the isotexture. The sol-gel structure has in the wavelength range from 450 nm to 1200 nm a smaller reflectance than the two-layer antireflection coating.

It can be seen that the isotexture shows the lowest reflectance over the complete wavelength range. In the range from 450 nm to 1200 nm the sol-gel structure has a slightly smaller reflectance than the two-layer ARC.

An OPTOS calculation of photo current densities (J_{ph}) of the different structures is used to investigate the potential of the sol-gel structure compared to the isotexture. A more detailed explanation, how OPTOS calculates the photo current densities of module stacks can be found in Tucher et al. [37]. For the calculation of J_{ph} in silicon, all interactions in the module stack were taken into account, which includes the 200 µm thick silicon substrate and a planar silver back reflector. With that the isotexture has the best J_{ph} of 41.2 mA/cm^2. For the sol-gel structure J_{ph} is 37.8 mA/cm^2. By integrating a lambertian scatterer at the back side of the silicon substrate the potential of perfect light trapping in combination with the sol-gel structure can be investigated. J_{ph} would in that case increase to 40.7 mA/cm^2, which is still lower than the J_{ph} for the isotexture without a lambertian scatterer.

Optics EXPRESS

In addition to this analysis we investigated the angle dependent performance of the structures in the module stack. The result is that the relative reduction of J_{ph} with increasing angle is similar for all structures. This is in accordance with earlier studies [38,39].

5. Conclusion and outlook

Within this work, simulation results for structured TiO_2 sol-gel layers on top of a silicon solar cell were presented. RCWA was used to simulate an encapsulated pillar structure for a broad set of different structure parameters.

An overview of the investigated different structure types and their relevant results is shown in Table 1.

Table 1. Conclusion of the different structure types investigated in this work and their best results.

structure type	period /nm	weighted reflection /%
sol-gel (half infinite front and back)	200	4.8
sol-gel (half infinite front and back) with binning of reflection into angles $< \vartheta$ (loss) & $> \vartheta$ (usable)	600	4.0
sol-gel in module (OPTOS calculation)	600	4.7
two-layer ARC (OPTOS calculation)		5.5
isotexture (OPTOS calculation)		2.3

It could be shown that for a simple model, where only the hemispherical reflectance at the solar cell front side was taken into account, the structure parameter proposed by Spinelli et al. [22] could be confirmed as optimal (detailed parameters see line 2 in Table 1). But in contrast to Spinelli it was established that these specific structures in encapsulation are no Mie scatterers, because they behave optically like a two-layer ARC.

However, for a full description of a module stack, interactions at the encapsulation-air-interface need to be taken into account. Then, the optimal structure parameters shifts towards larger periods, changing the working principle from an effective medium to a diffraction grating (detailed parameters see line 3 Table 1). As a result, part of the reflected light is diffracted and trapped in the module, leading to improved reflection behavior. Taking multiple interactions in the module into account by use of the OPTOS formalism, a comparison to an isotexture and a two-layer ARC was done. The reflection of the sol-gel structure is 0.8% lower than that of an optimized two-layer ARC (detailed parameters see line 4 and 5 Table 1). However, it is 2.4% higher than that of the isotexture (detailed parameters see line 4 and 6 Table 1) (detailed parameters see line 3 and 4 Table 1). What is more, for the sol-gel structure the photo current density in silicon compared to that of the isotexture is 8.3% lower, indicating that also the light trapping performance is not as good.

The structures investigated in this work were based on the research of Spinelli. There are more possibilities to shape the structure for example with continuous profiles [40], which represent more realistic results of a NIL process. Such structures will be investigated in future work.

Funding

German Federal Ministry of Economic Affairs and Energy (0324151A) (SOLGEL-PV); Deutsche Bundesstiftung Umwelt (DBU).

Acknowledgments

L. Stevens gratefully acknowledges scholarship support from the Deutsche Bundesstiftung Umwelt (DBU).

References

1. ITRPV, *International Technology Roadmap for Photovoltaic. 2016 Results, Eighth Edition (2017).*

Optics EXPRESS

2. M. A. Green, *High efficiency silicon solar cells* (Trans Tech Publications, 1987).
3. D. B. Lee, "Anisotropic Etching of Silicon," J. Appl. Phys. **40**(11), 4569–4574 (1969).
4. A. Hauser, I. Melnyk, P. Fath, S. Narayanan, S. Roberts, and T. M. Bruton, "A simplified process for isotropic texturing of mc-Si," in *Proceedings of the 3rd World Conference on Photovoltaic Energy Conversion* (2003), pp. 1447–1450.
5. H. Savin, P. Repo, G. von Gastrow, P. Ortega, E. Calle, M. Garín, and R. Alcubilla, "Black silicon solar cells with interdigitated back-contacts achieve 22.1% efficiency," Nat. Nanotechnol. **10**(7), 624–628 (2015).
6. J. Benick, A. Richter, R. Müller, H. Hauser, F. Feldmann, P. Krenckel, S. Riepe, F. Schindler, M. C. Schubert, M. Hermle, A. W. Bett, and S. W. Glunz, "High-Efficiency n-Type HP mc Silicon Solar Cells," IEEE J. Photovoltaics **7**(5), 1171–1175 (2017).
7. P. Panek, M. Lipinski, and J. Dutkiewicz, "Texturization of multicrystalline silicon by wet chemical etchinh for silicon solar cells," J. Mater. Sci. **40**(6), 1459–1463 (2005).
8. O. Schultz, S. W. Glunz, and G. P. Willeke, "Multicrystalline silicon solar cells exceeding 20% efficiency," Prog. Photovolt. Res. Appl. **12**(7), 553–558 (2004).
9. J. Nievendick, J. Specht, M. Zimmer, L. Zahner, W. Glover, D. Stüwe, D. Biro, and J. Rentsch, "An industrially applicable honeycomb texture," in *Proceedings of the 26th European Photovoltaic Solar Energy Conference and Exhibition (EUPVSEC)* (2011), pp. 1722–1725.
10. D. Niinobe, K. Nishimura, S. Matsuno, H. Fujioka, T. Katsura, T. Okamoto, T. Ishihara, H. Morikawa, and S. Arimoto, "Honeycomb-structured mulit-crystalline silicon solar cells with 18,6% efficiency via industrially applicable laser process," in *Proceedings of the 23rd European Photovoltaic Solar Energy Conference and Exhibition (EUPVSEC)* (2008).
11. H. Hauser, B. Michl, S. Schwarzkopf, V. Kübler, C. Müller, M. Hermle, and B. Bläsi, "Honeycomb texturing of Silicon via nanoimprint lithography for solar cell applications," IEEE J. Photovoltaics **2**(2), 114–122 (2012).
12. J. Thorstensen, J. Gjessing, E. S. Marstein, and S. E. Foss, "Light-Trapping Properties of a Diffractive Honeycomb Structure in Silicon," IEEE J. Photovoltaics **3**(2), 709–715 (2013).
13. K. X. Wang, Z. Yu, V. Liu, Y. Cui, and S. Fan, "Absorption Enhancement in Ultrathin Crystalline Silicon Solar Cells with Antireflection and Light-Trapping Nanocone Gratings," Nano Lett. **12**(3), 1616–1619 (2012).
14. A. Ingenito, O. Isabella, and M. Zeman, "Nano-cones on micro-pyramids. Modulated surface textures for maximal spectral response and high-efficiency solar cells," Prog. Photovolt. Res. Appl. **23**(11), 1649–1659 (2015).
15. M. L. Brongersma, Y. Cui, and S. Fan, "Light management for photovoltaics using high-index nanostructures," Nat. Mater. **13**(5), 451–460 (2014).
16. P. Spinelli, M. A. Verschuuren, and A. Polman, "Broadband omnidirectional antireflection coating based on subwavelength surface Mie resonators," Nat. Commun. **3**(1), 692 (2012).
17. A. Richter, J. Benick, and M. Hermle, "Boron Emitter Passivation With Al2O3 and Al2O3/SiN x Stacks Using ALD Al2O3," IEEE J. Photovolt **3**(1), 236–245 (2013).
18. P. Spinelli, B. Macco, M. A. Verschuuren, W. M. M. Kessels, and A. Polman, "Al2O3/TiO2 nano-pattern antireflection coating with ultralow surface recombination," Appl. Phys. Lett. **102**(23), 233902 (2013).
19. J. Eisenlohr, N. Tucher, B. G. Lee, O. Höhn, H. Hauser, J. Benick, B. Bläsi, M. Hermle, and J. C. Goldschmidt, "Diffractive Gratings for Light Trapping in Crystalline Silicon Solar Cells," in *OSA Light, Energy and the Environment Congress* (OSA, 2015), PTu4B.4.
20. J. Eisenlohr, N. Tucher, H. Hauser, M. Graf, J. Benick, B. Bläsi, J. C. Goldschmidt, and M. Hermle, "Efficiency increase of crystalline silicon solar cells with nanoimprinted rear side gratings for enhanced light trapping," Sol. Energy Mater. Sol. Cells **155**, 288–293 (2016).
21. R. Cariou, J. Benick, F. Feldmann, O. Höhn, H. Hauser, P. Beutel, N. Razek, M. Wimplinger, B. Bläsi, D. Lackner, M. Hermle, G. Siefer, S. W. Glunz, A. W. Bett, and F. Dimroth, "III–V-on-silicon solar cells reaching 33% photoconversion efficiency in two-terminal configuration," Nat. Energy **17**, 183 (2018).
22. P. Spinelli, F. Lenzmann, A. Weeber, and A. Polman, "Effect of EVA Encapsulation on Antireflection Properties of Mie Nanoscatterers for c-Si Solar Cells," IEEE J. Photovoltaics **5**(2), 559–564 (2015).
23. D. A. Goldman, J. Murray, and J. N. Munday, "Nanophotonic resonators for InP solar cells," Opt. Express **24**(10), A925–A934 (2016).
24. M. G. Moharam and T. K. Gaylord, "Diffraction analysis of dielectric surface-relief gratings," J. Opt. Soc. Am. **72**(10), 1385–1392 (1982).
25. K. Jäger, G. Köppel, D. Eisenhauer, D. Chen, M. Hammerschmidt, S. Burger, and C. Becker, "Optical simulations of advanced light management for liquid-phase crystallized silicon thin-film solar cells," in *Proc. of SPIE*, **10356** of Proceedings of SPIE (SPIE, 2017), p. 14.
26. N. Tucher, J. Eisenlohr, H. Gebrewold, P. Kiefel, O. Höhn, H. Hauser, J. C. Goldschmidt, and B. Bläsi, "Optical simulation of photovoltaic modules with multiple textured interfaces using the matrix-based formalism OPTOS," Opt. Express **24**(14), A1083–A1093 (2016).
27. L. Stevens, H. Hauser, O. Höhn, N. Tucher, C. Wellens, R. Jahn, W. Glaubitt, C. Müller, and B. Bläsi, "Nanoimprinted sol-gel materials for antireflective structures on silicon solar cells," in *Photonics for Solar Energy Systems VII* (SPIE, 2018), p. 10.
28. IEC, *Photovoltaic devices - part 3. measurement principles for terrestrial photovoltaic (PV) solar devices with reference spectral irradiance data.*, 2nd (International Electrotechnical Commission, 2008).

Optics EXPRESS

29. I. M. Peters, M. Rüdiger, H. Hauser, M. Hermle, and B. Bläsi, "Diffractive gratings for crystalline silicon solar cells-optimum parameters and loss mechanisms," Prog. Photovolt. Res. Appl. **20**(7), 862–873 (2012).
30. N. Tucher, B. Müller, P. Jakob, J. Eisenlohr, O. Höhn, H. Hauser, J. C. Goldschmidt, M. Hermle, and B. Bläsi, "Optical performance of the honeycomb texture – a cell and module level analysis using the OPTOS formalism," Sol. Energy Mater. Sol. Cells **173**, 66–71 (2017).
31. M. M. Braun and L. Pilon, "Effective optical properties of non-absorbing nanoporous thin films," Thin Solid Films **496**(2), 505–514 (2006).
32. A. Garahan, L. Pilon, J. Yin, and I. Saxena, "Effective optical properties of absorbing nanoporous and nanocomposite thin films," J. Appl. Phys. **101**(1), 014320 (2007).
33. D. J. Bergman, "The dielectric constant of a composite material-A problem in classical physics," Phys. Rep. **43** 377–407 (1978.).
34. J. R. Birchak, C. G. Gardner, J. E. Hipp, and J. M. Victor, "High dielectric constant microwave probes for sensing soil moisture," Proc. IEEE **62**(1), 93–98 (1974).
35. D. A. G. Bruggeman, "Berechnung verschiedener physikalischer Konstanten von heterogenen Substanzen. I. Dielektrizitätskonstanten und Leitfähigkeiten der Mischkörper aus isotropen Substanzen," Ann. Phys. **416**(7), 636–664 (1935).
36. C. Ballif, J. Dicker, D. Borchert, and T. Hofmann, "Solar glass with industrial porous SiO2 antireflection coating: measurements of photovoltaic module properties improvement and modelling of yearly energy yield gain," Sol. Energy Mater. Sol. Cells **82**(3), 331–344 (2004).
37. N. Tucher, J. Eisenlohr, P. Kiefel, H. Gebrewold, O. Höhn, H. Hauser, C. Müller, J. C. Goldschmidt, and B. Bläsi, "Efficient optical analysis of surface texture combinations for silicon solar cells," in *Proc. of SPIE*, Proceedings of SPIE (SPIE, 2016), 98980F.
38. I. Geisemeyer, N. Tucher, B. Muller, H. Steinkemper, J. Hohl-Ebinger, M. C. Schubert, and W. Warta, "Angle Dependence of Solar Cells and Modules. The Role of Cell Texturization," IEEE J. Photovoltaics **7**(1), 19–24 (2017).
39. I. Hädrich, M. Ernst, A. Thomson, P. Zheng, X. Zhang, H. Jin, and D. Macdonald, "How cell textures impact angular cell-to-module ratios and the annual yield of crystalline solar modules," Sol. Energy Mater. Sol. Cells **183**, 181–192 (2018).
40. J. Buencuerpo, L. Torné, R. Álvaro, J. M. Llorens, M. L. Dotor, and J. M. Ripalda, "Nano-cones for broadband light coupling to high index substrates," Sci. Rep. **6**(1), 38682 (2016).